Carbon-Nanotube−Electrolyte Interface: Quantum and Electric Double Layer Capacitance

Jinfeng Li,[†] Phi H. Q. Pham,[‡] Weiwei Zhou,[§] Ted D. Pham,[‖] and Peter J. Burke*[,‡,§,‖,⊥]

[†]Department of Physics and Astronomy, [‡]Department of Chemical Engineering and Materials Science, [§]Integrated Nanosystems Research Facility, [‖]Department of Biomedical Engineering, and [⊥]Department of Electrical Engineering and Computer Science, University of California, Irvine, California 92697, United States

🅢 Supporting Information

ABSTRACT: We present a comprehensive study of the electrochemical capacitance between a one-dimensional electronic material and an electrolyte. In contrast to a conventional, planar electrode, the nanoscale dimension of the electrode (with diameter smaller than the Debye length and approaching the size of the ions in solution) qualitatively changes the capacitance, which we measure and model herein. Furthermore, the finite density of states in these low dimensional electronic systems results in a quantum capacitance, which is comparable to the electrochemical capacitance. Using electrochemical impedance spectroscopy (EIS), we measure the ensemble average, complex, frequency dependent impedance (from 0.1 Hz to 1 MHz) between a purified (99.9%) semiconducting nanotube network and an aqueous electrolyte (KCl) at different concentrations between 10 mM and 1 M. The potential dependence of the capacitance is convoluted with the potential dependence of the in-plane conductance of the nanotube network, which we model using a transmission-line model to account for the frequency dependent in-plane impedance as well as the total interfacial impedance between the network and the electrolyte. The ionic strength dependence of the capacitance is expected to have a root cause from the double layer capacitance, which we model using a modified Poisson−Boltzmann equation. The relative contributions from those two capacitances can be quantitatively decoupled. We find a total capacitance per tube of 0.67−1.13 fF/μm according to liquid gate potential varying from −0.5 to −0.7 V.

KEYWORDS: carbon nanotubes, quantum capacitance, double layer, electrochemical impedance spectroscopy, Gouy−Chapman-Stern model, modified Poisson−Boltzmann equation
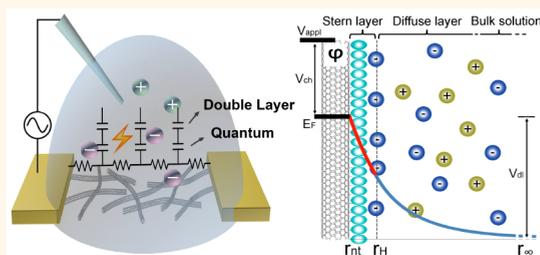
What is the capacitance between a 1d quantum wire (such as a carbon nanotube) and an electrolyte? This is probably the most fundamental scientific issue for any application where nanoelectrodes interface with electrolyte solutions, including for example electrochemical storage systems[1,2] (supercapacitors, batteries, fuel cells) and electronic interfaces with biological systems, such as chemical and biological sensors,[3] neural interfaces, and even electronic actuation of chemistry. Because of the reduced (almost atomic) size compared to traditional electrodes, as well as the low electronic density and quantum effects associated with the Pauli exclusion principle, the capacitance is theoretically expected to have comparable contributions from two significant phenomena: quantum and electrochemical.

One of the most fundamental questions in electrochemistry is, what is the capacitance between an electrode and an electrolyte? The electrochemical portion in planar geometries is well studied, and sophisticated models based on the now "textbook" Gouy−Chapman−Stern (GCS) model[4] which take

into account the effect of ion size[5] and varied Stern layer thickness[6] have been successful in describing a wide variety of electrode−electrolyte systems. However, with the modern advent of nanomaterials, a plethora of geometries are now available with electrodes with feature sizes (e.g., radius of curvature, pore size, *etc.*) smaller than the Debye length, even approaching the size of a solvated ion. In this case, profound differences from textbook GCS models are expected. What is traditional text book electrochemistry must be discarded, and new theories, driven by comprehensive, quantitative experimental data on model systems, will take their place.

As an example, in so-called nanoporous materials,[7−12] solution accessible caverns in amorphous, random materials provide a large effective surface area, hence potential

applications in supercapacitors. Researchers found that the capacitance per area diverges from classical, textbook GCS behavior when the average spacing ("pore") becomes of order 1 nm.[12−18] Here, in that context, "pore" is a random approaching of two electrode regions (positions where the cavern drops to a small value), not a cylindrical hole. Another example system is so-called nanotube paper,[19−21] where the nanotubes are treated as thin wires in a dense spaghetti, also with a large effective surface area. The nanotube paper should include multiple effects such as finite-radius of the nanotubes, as well as other non-GCS effects when nanotube spacing becomes comparable to the Debye length, in analogy with the nanoporous materials. However, due in part to the complexity of the geometry and the electrochemistry, to our knowledge, no such a comprehensive study has been performed, leaving open the possibility of improved nanotube paper supercapacitors if the fundamental underlying science of the electrochemistry can be understood.

An additional significant effect, that of the quantum capacitance, has not been well considered in the context of either nanoporous materials or nanotube paper. The quantum capacitance arises from system's low density of states near the Fermi level,[22] and has been studied in a dry environment.[23] Its effect on the electrical behavior of the capacitance between a material with small radius of curvature and an electrolyte solution has not been well studied, although it has been demonstrated in planar large area graphene electrodes[24,25] with essentially infinite radius of curvature, where the classical textbook GCS describes well the electrochemical capacitance.

In order to elucidate the contributions of the small radius of curvature on electrode−electrolyte capacitance in a well-controlled, model system, as well as study the effects and significance of the quantum capacitance, we have chosen a model system with well understood, well controlled radius of curvature and constant (rather than random) cylindrical geometry, that of a sparse array of carbon nanotubes horizontally distributed on a solid (insulating) surface. In this limit, the nanotube−nanotube spacing is much larger than the Debye length, allowing us to treat each nanotube individually. We assume the electrolyte does not penetrate to the inside of the nanotube, so each nanotube is treated as a solid cylinder electrode. (The effect would be small even if it did, which we discuss in detail in the main manuscript below.) In contrast to the nanoporous materials, which have a fractal 3d like geometry, this geometry enables us to carefully study the effects of quantum capacitance and small radius of curvature in one system. A priori, in this system, both the quantum capacitance and the double layer capacitance are comparable in value and interact with each other. One or the other can dominate the total capacitance, depending on the detailed parameters such as ionic strength and applied potential.

This fundamental study is the first step toward a more comprehensive understanding of the dense limit, that of nanotube paper, which is beyond the scope of this paper. However, as this is the fundamental, scientific study of the electrochemical and quantum capacitance of a nanocylinder geometry, it is expected to have applications in many fields beyond supercapacitors.

With this in mind, here we present quantitative measurements and models of the capacitance between carbon nanotubes and an electrolyte, including developing a comprehensive, and quantitative model for 1d quantum wire

to electrolyte electrochemical capacitance as well as the relative magnitude of both the electrochemical capacitance, and the quantum capacitance in liquid. To do this, we measure the differential capacitance between single-walled carbon nanotubes (SWNTs) and electrolyte solution, using a semiconducting SWNT network. To ascertain the various contributions to this total interfacial capacitance, we use electrochemical impedance spectroscopy (EIS) to determine the ensemble average, complex, frequency dependent impedance (from 0.1 Hz to 1 MHz) between a purified (99.9%) semiconducting nanotube network and an aqueous electrolyte (KCl) at different concentrations between 10 mM and 1 M. By the interfacial capacitance, we mean the total capacitance, which includes contributions from both the quantum and double layer capacitance in series. We find a total capacitance per tube of order 1 fF/μm and map its dependence on bias and electrolyte strength. This fundamental and experimental study of the total capacitance between a 1d material and an electrolyte provides a comprehensive scientific foundation for understanding interactions between any 1d electronic system and liquid electrolytes, a growing area of research for a variety of fields from energy to biology.

RESULTS AND DISCUSSION

Device Description and Measurement Configuration. Figure 1 shows a schematic of the measurement setup using a thin film transistor type device with SWNT networks as the semiconducting channel. The upper panel shows the optical and the scanning electron microscopy (SEM) images of the
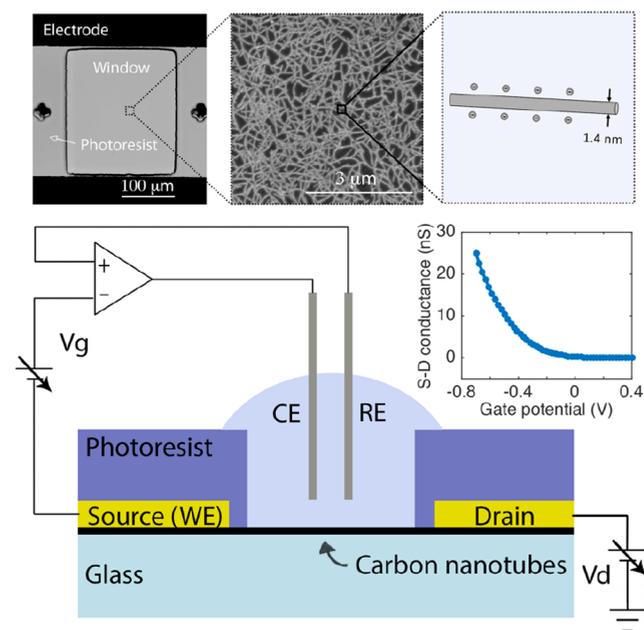

Figure 1. Single-walled carbon nanotube (SWNT) network device illustration and measurement configuration. Schematic of the interfacial impedance measurement of the SWNT network on an inert glass substrate with source and drain electrodes covered by photoresist and the channel exposed to electrolyte solution. The nanotube network channel is liquid gated by an aqueous electrode, and the impedance of the SWNT−electrolyte interface is measured with an AC perturbation added on the gate potential. The upper panel shows the optical micrograph of the device, the SEM image of the nanotube network, the geometry of SWNTs, and the transfer characteristic of the device.

actual device, along with a diagram of the geometry of the SWNTs, and the DC conductance characteristic. The device fabrication is detailed in the Methods section. Briefly, a SWNT network is transferred to an inert glass substrate with Au electrodes deposited on two sides as the source and drain electrodes, with channel length varying from 40 to 300 μm and a fixed width of 200 μm. Standard photolithography was used to insulate the electrodes, while exposing the SWNTs to solution through a photoresist window. Using glass as substrate instead of Si/SiO$_2$ wafer minimizes the background capacitance. The exposed SWNTs have relatively high density ($\sim$12 SWNTs/μm^2) and form a uniform random network,[26] as shown in the SEM image, ensuring a good current pathway between the source and drain electrodes.

An ionic solution consisting of 10 mM to 1 M potassium chloride contacts the SWNTs through the exposed window and is used as a "solution gate". The gate potential is controlled and varied using a potentiostat (Gamry Reference 600) with a standard three-electrode electrochemical configuration[4] as shown in Figure 1. Here the SWNTs act as the working electrode (WE), and are controlled with respect to the Ag/AgCl reference electrode (RE) and a platinum counter electrode (CE). The gate potential window is limited to between −0.7 V (SWNTs in an on-state) and 0.4 V (SWNTs in an off-state) to avoid water oxidation at the SWNTs surface. As there are no active redox species in the potential range in the solution, we expect only trace redox (Faradaic) currents, allowing us to isolate the capacitance exclusively. A small AC perturbation (10 mV, 0.1 Hz to 1 MHz) was superimposed onto the gate potential and the current response was measured to determine the frequency dependent impedance information on the SWNT−electrolyte interface. Before the impedance measurement, the in-plane source-drain conductance of the SWNT network as a function of gate potential was characterized using a source measurement unit.

DC Characteristics. The conductance curve in Figure 1 shows the transfer characteristics of the SWNT network with length 250 μm and width 200 μm. It is a typical p-type depletion curve with source-drain conductance as a function of liquid gate potential, measured by sweeping the gate potential from −0.7 to 0.4 V at a fixed source-drain bias 100 mV. The on/off ratio is $\sim$1000, demonstrating that the network is dominated by semiconducting SWNTs. This "background current" (see the Supporting Information), may be nonzero due to redox reactions with trace impurities in the electrolyte. This term is sometimes called "leakage current", using the language of semiconductors where the liquid is serving as the gate. The (DC) leakage current between the electrolyte and the SWNT film is negligible compared to the (DC) source-drain current, confirming the interpretation that only capacitive current flows between the SWNT film and the electrolyte in our experiments. This enables us to accurately determine the DC in-plane SWNTs conductance and focus on the interface capacitance.

Capacitance Measurement at 10 Hz. In order to determine the impedance (hence capacitance) between the SWNT network and the electrolyte, a small AC perturbation at 10 Hz was added to the gate potential and the in phase 10 Hz current was measured with a lock-in analyzer. At sufficiently low frequencies the system can be modeled as a simple capacitor (discussed in more detail later). The capacitance can be determined from the measured impedance using the relationship $C \equiv -1/\omega Z_{img}$. Figure 2a shows the measured
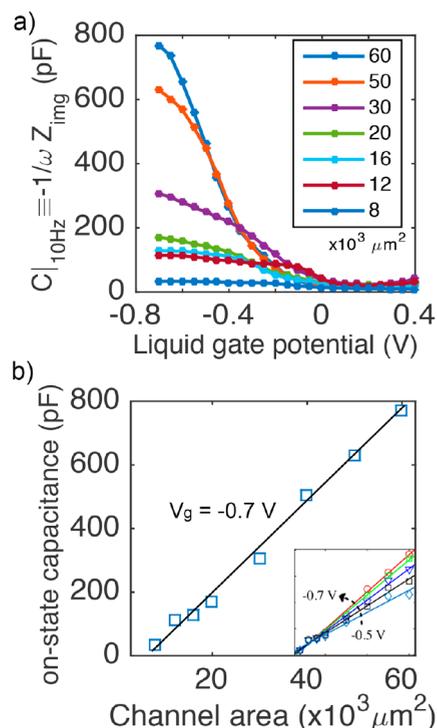

Figure 2. SWNT network-to-electrolyte capacitance with different channel areas measured at a single frequency 10 Hz. (a) Capacitance curves as functions of liquid gate potential with varied channel areas, measured on the same sheet of SWNT network film to ensure consistence of SWNT density. (b) Linear relationship between the on-state capacitance and the corresponding channel areas at gate potential −0.7 V, and over a range of gate potentials in the inset.

capacitances of various devices with different channel areas on the same chip. Within the positive gate potential window where most SWNTs are in the off-state, there is a parasitic capacitance $\sim$20 pF. As the SWNTs turn on gradually, the capacitances trend to saturate and show a clear correlation with the channel area. Figure 2b shows the capacitance scales in a linear trend with the channel area at gate potentials −0.7 V. The slope of the correlation gives the capacitance area density at values 14.2 fF/μm^2. The linearity remains over the range of gate potential between −0.5 and −0.7 V, corresponding to the capacitance value of 8.4−14.2 fF/μm^2 (inset of Figure 2b).

Using this measured capacitance density and the known SWNT density and average length, we can determine the capacitance per unit length of a single nanotube. We estimate the density of SWNTs to be 12.6 SWNTs/μm^2 (see Supporting Information Note 4) and mean length of 1 μm. This gives us an estimated value of 0.67−1.13 fF/μm (inset of Figure 8) for the total interfacial capacitance between SWNTs and electrolyte with dependence on the gate potential.

Effect of In-Plane Conductance. For more quantitative studies, we must take into account the in-plane conductance of the SWNT network. Although a single frequency measurement provides some insight, EIS is a much more powerful tool to characterize the system over a broad range of frequencies. Figure 3 shows the measured impedance spectrum of the same device, where the red curves correspond to the on-state impedance spectrum with gate potential at −0.7 V and the blue curves correspond to the off-state impedance spectrum with gate potential at 0.2 V. In the off-state, the nanotubes are not
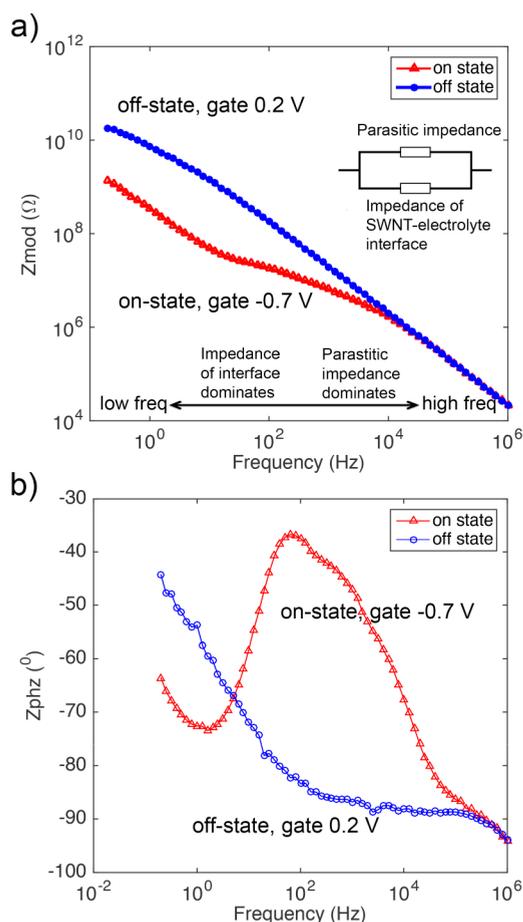
Figure 3. Experimental EIS Bode plot of the SWNT−electrolyte interface. Impedance spectra measured at off-state (blue curve) and on-state (red curve) are plotted with (a) impedance modulus vs frequency and (b) impedance phase vs frequency. The inset circuit demonstrates the parallel relationship between the parasitic impedance and the impedance of interest.
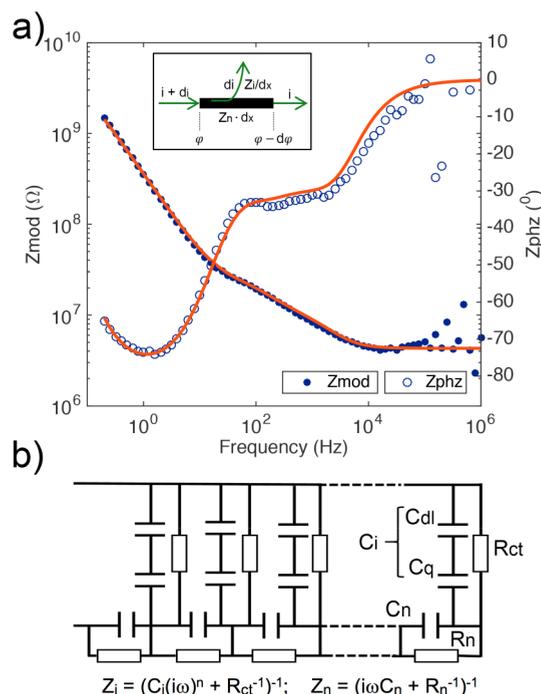

Figure 4. Transmission line modeling of the impedance spectrum. (a) Impedance spectrum after subtracting parasitic impedance, fitted by a modified transmission line (TL) model. The inset shows the potential and current variations of a differential length of SWNT network channel. (b) Circuit representation of the transmission line model.

conducting, so the only impedance measured is the parasitic impedance between the contact electrodes and the electrolyte. Independent experiments show that this parasitic impedance scales linearly with the area of the contact electrodes confirming this interpretation (see Supporting Information Note 6). Also, at high frequencies, the parasitic impedance dominates, and the on-state and off-state curves merge, as expected. Since we have measured the complete, complex impedance, we can subtract the parasitic impedance to determine the SWNT−electrolyte impedance using

$$Z_{\text{SWNT−electrolyte}} = Z_{\text{measured}} − Z_{\text{parasitic}}$$

where $Z_{\text{parasitic}}$ is determined using the off-state or high-frequency measured impedance.

We plot the impedance spectrum of the SWNT−electrolyte interface in Figure 4a determined using this procedure. In contrast to most electrochemical experiments, in our experiments, the in-plane conductance of the nanotubes can be lower than the capacitive impedance between the SWNT network and the electrolyte. Therefore, $Z_{\text{SWNT−electrolye}}$ also includes contributions from the in-plane conductance which must be taken into account. In order to do this, we model the system as a distributed in plane and capacitive network ("transmission line", although only Rs and Cs so not like a wave), which

includes both the in-plane impedance of the nanotube network, as well as the network-to-solution impedance. In Figure 4b, we diagram the distributed model, which contains all of the important elements: capacitance between the network and the electrolyte, faradaic (redox) impedance between the nanotube network and the electrolyte, in-plane conductance of the nanotube network, and in-plane capacitance of the nanotube network. Using this model, we can apply the standard telegraph equations from transmission line theory to find the following relationship between the total (measured) impedance Z and the length of the system as well as the individual components:[27]

$$Z = \frac{\varphi(0)}{i(0)} = (Z_i Z_n)^{1/2} \coth[L(Z_n/Z_i)^{1/2}] \tag{1}$$

where L is the channel length of the SWNTs thin film transistor, Z_i is the complex impedance per unit length (Ω m^{-1}) of the interface, and Z_n is the in-plane impedance length (Ω m) of the SWNT network, shown in the Figure 4b.

The impedance of SWNT−electrolyte interface Z_i has components of resistance and capacitance in parallel. The resistance R_{ct} is due to trace Faradaic current; the capacitance C_i is a combination of double layer capacitance and quantum capacitance.[28] An R||C circuit model can intuitively describe the impedance of different types of interfaces; however, experimentally, the interface impedance commonly shows a nonideal capacitance phenomenon[29] with a phase shift at different values from −90°. As we can see in Figure 4a, in the low frequency range, the phase part of the impedance goes to ∼ −80°, suggesting a nonideal phase shift of the interface capacitance. A phenomenological constant phase element (CPE),[30−32] $Z_{\text{CPE}} = 1/C_i(i\omega)^n$, is commonly used to substitute

the interface capacitance with adjustment of phase shift to a value of $-(90n)°$. The parameter n describes the purity of the capacitance with range from 0 to 1. The overall impedance of the SWNT−electrolyte interface therefore can be formulated as

$$Z_i = \frac{R_{ct}}{1 + C_i(i\omega)^n R_{ct}} \tag{2}$$

The in-plane impedance Z_n of the SWNT network along the TFT channel is gate potential dependent. Its resistance component R_n comes from the SWNTs' intrinsic resistance, cross-junction resistance, and the geometry of the networks (corresponding to the source-drain conductance measured previously). Besides the resistance component, the electrostatic coupling between SWNTs and SWNTs forms a capacitance C_n that is in parallel with the resistance. Since the sweep potential in the interfacial capacitance measurement is a small perturbation added on the gate potential, for a given gate potential E_g, the impedance of the SWNT network can be expressed as

$$Z_n|_{E_g} = \frac{R_n}{1 + C_n i\omega R_n} \tag{3}$$

By combining the eqs 1−3, the theoretical expression to model the impedance of SWNT−electrolyte interface is

$$Z = R_c + \sqrt{\frac{R_{ct}R_n}{(1 + (i\omega)^n C_i R_{ct})(1 + i\omega C_n R_n)}}$$
$$\times \coth\left[L\sqrt{\frac{R_n(1 + (i\omega)^n C_i R_{ct})}{R_{ct} + i\omega C_n R_{ct} R_n}}\right] \tag{4}$$

where R_c is added to represent the series resistances that include bulk solution resistance, electrode contact resistance, and resistance of nongated SWNTs covered under photoresist.

We performed a fit of eq 4 to the impedance spectrum data with the following as parameters (R_{ct}, C_i, R_n, C_n, n, R_c). The resultant fit describes the data well over the entire frequency spectrum as seen in Figure 4a. Using this fit, we can obtain a quantitative value for the components in the SWNT network system. These results are shown in Table 1.

Table 1. Total Interfacial Capacitance Density, Capacitance Purity, Charge Transfer Resistance-Area, In-Plane Sheet Capacitance, and Sheet Resistance of the SWNT Network, Estimated by Fitting the TL Model to the Experimental Spectrum

C_i (fF/μm^2)	n	R_{ct} (MΩ·mm^2)	C_n (pF/sq)	R_n (MΩ/sq)	R_c (MΩ)
11.5	0.9	247.5	1.7	39.8	4.3

The fitted in-plane resistance of SWNT network along the whole channel is 49.7 MΩ, in good agreement with the DC-measured value a 40 MΩ. The in-plane capacitance is small, as expected. The faradaic resistance (due to redox reactions with trace impurities in the electrolyte) is also high, as expected, and consistent with the DC measured "leakage current". The quality of the curve fit and the agreement with the DC data adds additional confidence when assessing the interfacial impedance. We find an estimated total interfacial capacitance is 11.5 fF/μm^2, comparable to but a more quantitative measure than the 10 Hz estimation provided above. This demonstrates

the need to perform a more comprehensive measurement of the total impedance spectrum opposed to simply measuring the impedance at a single frequency. The EIS measurement yields an estimated capacitance per length of 0.9 fF/μm at gate potential -0.7 V, consistent with the rough estimate from the 10 Hz capacitance, which neglected the transmission line effects discussed above.

We now discuss the low frequency limit (claimed as 10 Hz above) in more detail, and relate it to the transmission line impedance model. Since the charge-transfer resistance R_{ct} is significantly larger than the in-plane resistance R_n, in the on-state, the low frequency regime ($\omega \rightarrow 0$) leads to

$$\lim_{\substack{\omega \rightarrow 0 \\ R_{ct} \gg R_n}} \frac{\partial Z}{\partial \omega} = \frac{\partial Z_{Randles}}{\partial \omega} \tag{5}$$

where $Z_{Randles}$ is the impedance of a Randles circuit model[4] containing a resistor in series with a parallel combination of a capacitor and a resistor. The overall impedance can be approximated to first order as a Randles circuit. Further simplification can be made when the charge transfer resistance is significantly larger than the capacitive impedance at the measurement frequency 10 Hz, i.e., $\omega C_i R_{ct} \gg 1$, such that the impact of the charge transfer resistance is insignificant. With all of the above assumptions, the transmission-line model can be approximated as a simple circuit model with the total interfacial capacitance in series with other resistive elements. This explains the good agreement between the 10 Hz measured capacitance and the more refined transmission line model measurement.

Quantum vs Electrochemical Capacitance. The measured capacitance between the SWNT network and the electrolyte comes from two physical properties: the finite density of states (DOS) of the SWNT and the double layer structure of the SWNT−electrolyte interface. These two types of capacitances come from two different physical mechanisms, and form the total interfacial capacitance in series (see circuit diagram in Figure 5), given by $1/C_i = 1/C_q + 1/C_{dl}$, with the smaller of the two capacitances dominating the total capacitance.[28] The series capacitance model is an approximation which ignores the charge transfer effect and contact-induced band bending. This point is discussed in more detail below in the section Series Model Approximation.

Now that we have measured the capacitance, we are in a position to determine: *Which capacitance dominates, the electrochemical (double layer) or the quantum capacitance?* In order to answer that question, we need more sophisticated models of each capacitance, which we develop in detail below. In general, the applied voltage (V_{appl}) will be divided unevenly between the two capacitances. Furthermore, each capacitance contribution is dependent on the potential drop across that particular capacitor, *i.e.*, the value of C_{dl} depends on the potential drop across C_{dl}. Similarly, the value of C_q depends (and only depends) on the potential drop across C_q which we call V_{ch} (the change of chemical potential). However, the way in which the total voltage is divided depends on the values of the individual capacitances, so they must all be determined self-consistently, once a suitable model for $C_{dl}(V_{dl})$ and $C_q(V_{ch})$ is determined. This is further complicated because C_{dl} depends also on ionic strength whereas C_q is not expected to depend on ionic strength.

The detailed models for $C_{dl}(V_{dl})$ and $C_q(V_{ch})$ are presented below in turn. For now, we summarize the results of these
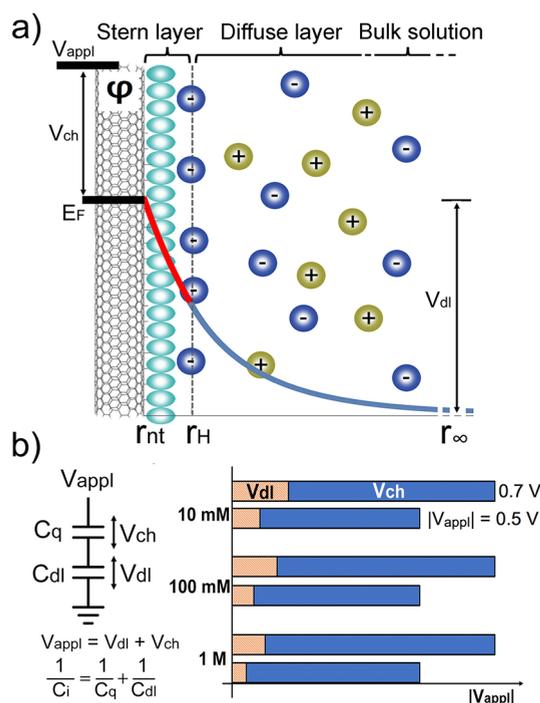
Figure 5. Potential drop across the SWNT−electrolyte interface. (a) Schematic of the double layer structure at the SWNT surface. The potential distribution along the radial direction consists of the chemical potential shift (V_{ch}), followed the decay in the Stern layer (red), and the diffuse layer (blue). (b) Relative contribution of each potential drop (V_{ch} and V_{dl}) to the total potential drop, which is equal to the applied potential (V_{appl}) at three different ionic strengths, 10 mM, 100 mM, and 1 M.

findings in Figure 5, which shows the relative potential drop across each component at three different ionic concentrations. Two conclusions can be drawn from this. First, the potential is mostly dropped across the V_{ch} in all configurations. This indicates that the quantum capacitance actually dominates in most cases. Second, V_{ch} varies as the ionic concentration changes. As a result, the quantum capacitance has an indirect dependence on the ionic concentration. We now turn to a detailed discussion of each component.

Double Layer Model of a SWNT. In this section, we model the double layer for the case of a carbon nanotube geometry based on the GCS model using a modified Poisson−Boltzmann (PB) equation. Initial models in the cylindrical geometry have taken into account the effect of small radius of curvature on the diffuse capacitance of carbon nanotubes and monatomic wires,[33,34] but the ion size, correlation, Stern layer thickness, and close packing issues were not incorporated, which we find is a critical effect to include in order to provide a realistic model for our data. We are particularly interested in extracting the voltage dependence of the double layer capacitance (i.e., $C_{dl}(V_{dl})$), as well as the effect of ionic strength.

The electric double layer of the electrode−electrolyte interface was first modeled by Helmholtz as a two-plate capacitor, with the metal electrode and electrolyte electrode separated by a certain distance caused by finite ion size (Figure 6a). Gouy and Chapman improved the model by considering the electrolyte side as the diffusive structure of counterions loosely accumulated to the metal electrode surface (Figure 6b). Later, Stern combined the Helmholtz model and Gouy−Chapman model, and described the double layer as two capacitances in series: the Helmholtz's plate capacitance in series with the Gouy−Chapman's diffuse capacitance (Figure 6c).[4] The GCS model has become the popular model for the electric double layer. Modern electrochemistry theories still use the GCS model as a framework but include more effects such as the finite ion size and short-range correlations to approach the real system. The Poisson−Boltzmann (PB) equation (Debye−Hückel theory) and the mean sphere approximation (MSA) are two popular approaches adapted to calculate the properties of realistic electrolyte systems.[35,36] The original PB methods treat ions as point charges in a continuous dielectric medium and ignore the short-range correlation of ions, which provides a limiting prediction, valid at low concentrations. MSA overcomes this limitation being able to work well in strong electrolytes, by modeling ions as hard charges spheres in a continuous medium, and includes the correlation effect. Modified PB methods (used in this paper) can also account for the effect of nonzero ion size and close-range correlation, which is easier to compute and can provide approximately the same level of accuracy as MSA. More advanced methods such
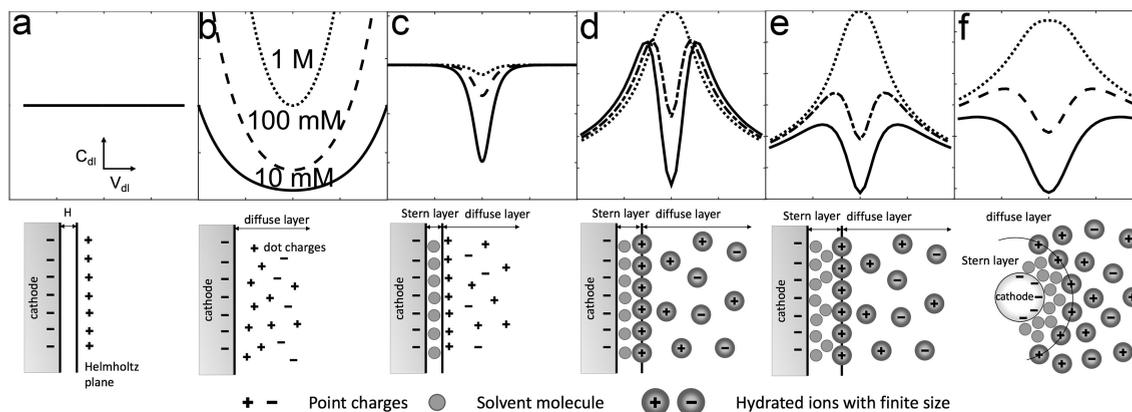

Figure 6. Evolution of the electric double layer models. Top panel: capacitance vs potential $C_{dl}(V_{dl})$ at different ionic concentrations. Bottom panel: the arrangement of solvated ions near the interface. (a) Helmholtz model, (b) Gouy−Chapman model, (c) Gouy−Chapman-Stern (GCS) model, (d) GCS model with the effect of ion size, (e) including the effect of varied Stern layer thickness, and (f) applied to SWNT nanoelectrode with extreme curvature.

as classical molecular dynamics (MD) simulations and DFT-based *ab initio* MD simulations,[37−39] which treat the medium as discrete molecules with realistic intermolecular correlations, provide a more detailed model for the system, especially for multivalent molecules. However, MD methods require large computational power.

The effect of finite ion size and the effect of Stern layer thickness on the GCS model creates a more complex $C_{dl}(V_{dl})$ curve, as shown in Figure 6d and e. While these effects have been well studied in refs 5, 6, and 40 and the resultant prediction is qualitatively different from that of GCS model, they are usually neglected under limited conditions when the curvature of electrode is small, ionic concentration is low and electrode surface potential is low. However, here in the case of a carbon nanotube, none of above conditions are valid, and hence all these three effects must be taken into account. In addition, SWNTs have cylindrical geometry with extreme convex surface, the geometrical effect provides larger diffusion space and adds quantitative distinction to the final results such as the change of slope in the decreasing trend of the diffusion capacitance at high electrode surface potential, indicated schematically in Figure 6f. We now turn to our detailed model for the nanotube electrolyte capacitance which includes all those effects.

Figure 5a shows the double layer structure based on the GCS model.[4,41] Near the surface of the charged SWNT electrode, electrostatic interactions cause counterions to accumulate to the surface of the electrode, forming a compact Stern layer and a loose diffuse layer. In the Stern layer, the compacted layer of counterions strongly attaches to the electrode surface with solvent molecules between them. The solvent molecule can be considered as the hydration shell of the electrode, whose thickness changes according to ionic concentration. In the diffuse layer, free ions with thermally activated movement loosely accumulate near the Stern layer under the influence of electrostatic force. The accumulation of counterions in these two layers electrically screens the electrode surface, resulting in electric potential decaying exponentially to zero from the surface to the bulk solution.

Ionic species in the solution are governed by motion dynamics that has a coupled influence from diffusion and electrostatic forces. This behavior can be described by the convection−diffusion equation together with Poisson's equation. From these two equations, and considering both equilibrium state and binary symmetric electrolytes, the potential distribution can be accounted for by the original Poisson−Boltzmann equation:[4]

$$\nabla \cdot (\varepsilon_r \varepsilon_0 \nabla \varphi) = 2\rho_q \sinh\left(\frac{q\varphi}{k_B T}\right) \tag{6}$$

where φ is the electric potential distribution in space, $\rho_q = qN_A c_0$ is the charge density of cation or anion in a symmetric electrolyte solution, c_0 is the molar concentration of ion species, N_A is Avogadro's constant, and $q = ze$ is the charge of the ions with valence z and the electron charge e.

A modification of the Poisson−Boltzmann can be made to account for the short-range correlation:[42]

$$\nabla \cdot (\varepsilon_r \varepsilon_0 \nabla \varphi) = 2\rho_q \sinh\left(\alpha \frac{q\varphi}{k_B T}\right) \tag{7}$$

which only defers from the original PB equation by rescaling the potential dependence with the correlation parameter α.

For a planar electrode, there is an analytic solution for the Poisson−Boltzmann equation, which can give the double layer capacitance,[4]

$$\frac{1}{C_{dl}} = \frac{1}{C_{Stern}} + \frac{1}{C_{diffuse}}$$
$$= \frac{d_s}{\varepsilon_r \varepsilon_0} + \frac{1}{(2\varepsilon_r \varepsilon_0 ze\rho_q \alpha / k_B T)^{1/2} \cosh(ze\varphi_H \alpha / 2k_B T)} \tag{8}$$

where C_{Stern} is the capacitance of the Stern layer, $C_{diffuse}$ is the capacitance of the diffuse layer, d_s is the thickness of the Stern layer, and φ_H is the potential at the outer Helmholtz plane ($r = r_H$ plane in Figure 5a).

For a SWNT electrode, one can treat it as a solid cylindrical electrode, and estimate the double layer capacitance by solving the Poisson−Boltzmann equation numerically in cylindrical coordinates. Though the inner tubular pore of a nanotube also stores charges,[43−49] we ignore this part because the *differential* capacitance of it is small due to narrow confinement and vanishes over a threshold gating potential.[16] The differential capacitance is small because, once the inner portion of the nanotube is filled up with ionic charge, it is "full", and adding additional voltage will not increase the charge. A calculation of diffuse layer capacitance only (neglecting the Stern layer) of carbon nanotube has been reported in ref 33. However, as we will see below, the Stern layer is nontrivial, and cannot be neglected in this calculation. In the case of high ionic concentration and high electrode potential, additional assumptions are necessary in order to account for the effect of finite ion size and Stern layer thickness.

A second modification of the Poisson−Boltzmann equation[5,50,51] can be made to account for the finite ion size by setting a maximum limit of the local ion density, and for the Stern layer by setting a plane where charged ions cannot pass through. The Stern layer thickness is chosen according to ionic concentrations, based on hydrated ion radius and reported experiment data.[6,52] For the cylindrical geometry of SWNTs, the modified model can be expressed below,[5,53]

$$\frac{1}{r}\frac{d}{dr}\left(\varepsilon_r \varepsilon_0 r \frac{d}{dr}\right)\varphi = \begin{cases} 0, & r_{nt} \leq r \leq r_H \\ \dfrac{2\rho_q \sinh\left(\alpha \frac{q\varphi}{k_B T}\right)}{1 + 2\nu \sinh^2\left(\alpha \frac{q\varphi}{2k_B T}\right)}, & r \geq r_H \end{cases} \tag{9}$$

where the additional parameters is ν, the packing parameter[5,53] defined as $\nu = 2a^3 N_A c_\infty = 2c_\infty / c_{max}$, related to the ratio between the ionic concentration in bulk solution and the local maximum ionic concentration. Within the Stern layer ($r_{nt} < r < r_H$), there is no free charge distribution; the Poisson equation is set to zero. The potential at the electrode surface is the applied potential φ_0, and the potential in the bulk solution decays to zero. Potential and electric force should be continuous at the outer Helmholtz plane (considering a constant electric permittivity). These give us a list of boundary conditions: $\varphi(r = r_{nt}) = \varphi_0$, $\varphi(r = +\infty) = 0$, and $E_{r1-} = E_{r1+}$, $\varphi_{r1-} = \varphi_{r1+}$.

To solve eq 9, the essential parameters are chosen to best characterize the present experiment: T = 298 K, electric permittivity ε_r = 80.2 for water at room temperature, effective

hydrated ion radius[52] of Cl^- and K^+ r_{ion} = 0.33 nm, the mean van der Waals distance between water molecules d_w = 0.31 nm, the Stern layer thickness d_s = 0.9 and 0.62 nm for electrolyte concentration at 1 mM and 10 mM, and reaches the limit of ion's hydrated radius at higher concentrations,[4,6] the average SWNT radius r_{nt} = 0.7 nm. The correlation parameter α is estimated to be 0.9997 according to the definition in ref. [42], showing a minor correlation effect (α = 1 means no correlation effect). Using these numerical values and the boundary conditions, COMSOL 5.1 is applied to solve eq 9 at various applied potentials and ionic concentrations. The resulting potential distribution along the radial direction of SWNT exponentially decays from the SWNT surface to the bulk solution as expected. The Debye screening length varies from 1 to 10 nm dependent on the electrode potential and electrolyte concentrations. From the potential distribution, the electrically stored charge Q in SWNT can be calculated according to Gauss's law (see Supporting Information Note 3), and therefore, we can calculate the differential capacitance of the double layer: $C = dQ/d\varphi_0$. Here φ_0 is the same as the potential V_{dl} in Figure 5.

The resulting double layer capacitance of SWNTs as a function of the electrode potential is shown in Figure 7. It is
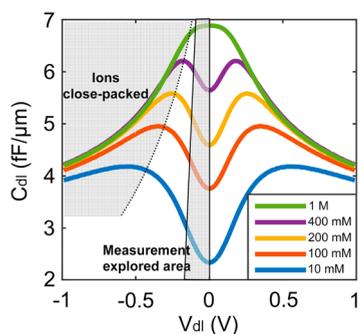

Figure 7. Double layer capacitance of a SWNT as a function of surface potential and ionic concentration. Ions are close-packed near the SWNT when either the surface potential or the ionic concentration is high (top left gray area). The measurement here only covers the double layer capacitance in a low potential range (middle gray area), due to the domination of quantum capacitance.

symmetric, since we used a binary symmetric electrolyte with similar hydrated radius of cations and anions. The close-packing configuration of ions happens at high surface potential or high ionic concentration. As the surface potential increases, the double layer capacitance first increases and then decreases. The change of trend happens at a point where ions are close-packed near the electrode surface. Before reaching the close packing point, the increasing electric field will compact the Stern layer and diffuse layers to make the double layer thinner, which increases the double layer capacitance. Continuing increasing the electric field beyond the close-packing point, instead of getting thinner, the Stern layer and diffuse layer get crowded and grow quickly in thickness (ions are close-packed). Inversely proportional to the thickness, the double layer capacitance starts to decrease. This change of trend happens earlier in higher ionic concentration and eventually vanishes and only the decrease trend shows (e.g., the 1 M case in Figure 7). The decrease trend will softly level off and the double layer capacitance becomes independent of ionic concentration,

which happens as the growth of double layer in thickness balances with the growth of the ion-packed electrode in surface area. Ion distribution near the electrode surface is the result of balanced forces caused by potential gradient and concentration gradients, hence changing ionic concentration should have a similar effect as changing electrode surface potential. Close-packing of ions can happen at high ionic concentration, even when the surface potential is low (see Supporting Information Note 7).

Although we explored the SWNT-to-electrolyte capacitance over a wide range of applied potential −0.7 ∼ 0.4 V, the potential drop on the double layer during the measurement is within a small range as shown in the middle gray area in Figure 7. A majority of the applied potential is on the change of chemical potential of SWNTs. Hence, in the limited window of measurement, we did not reach the close-packing condition of ions. In the calculation, we used the hydrated ion size as the minimum distance between ions, however the distance can be larger due to the dielectrophoretic repulsion of ions.[40] In this case, C_{dl} can start to decrease at smaller surface potential. A strong electric field has influence on the dielectric constant of the Stern layer.[5] When the electric field is larger than ∼25 V/nm, the field dependent dielectric constant of Stern layer need to be considered for more accurate estimation.[54]

Quantum Capacitance. Although the quantum capacitance has been studied in a dry environment[23] and the principles are well-understood, it is important to develop a model for our particular nanotube diameter distribution and voltage range to adequately ascertain its contribution to the total capacitance in a liquid electrolyte environment, which has not (until now) been measured. We now perform such a calculation.

The quantum capacitance originating from the finite density of states (DOS) of SWNTs is on the order of $C_q^0 = 4e^2/\pi\hbar\nu_F$ ≈ 0.4 fF/μm for one sub-band occupied.[22] In the case of higher chemical potential with the second sub-band occupied, this value can be larger. Here, in the configuration of electrolyte gating, ions closely interacting with SWNTs can very effectively shift the chemical potential of SWNTs. We expect ∼1 fF/ μm will hold in the case of electrolyte gated SWNTs. Reference 23 has measured the quantum capacitance of a SiO_x-gated SWNT in dry environment. A detailed comparison of the measurement data between the reference work and this work is included in Supporting Information Note 1.

Theory of Ensemble Averaged Quantum Capacitance. For quantum capacitance of individual semiconducting SWNTs, its value as a function of chemical potential and tube diameter is given by[23,55]

$$C_q(\mu, d) = \int_{sub-band} dE \, F_T(E - \mu) C_q^0 \sum_{j=-3}^{3} \left(1 - (E_j/E)^2\right)^{-1/2}$$

$$E_j = \hbar\nu_F \frac{2j}{3d}$$

$$(10)$$

where $F_T(E) = (4k_BT)^{-1} \text{sech}^2(E/2k_BT)$ is thermal broadening function, k_B is the Boltzmann constant, T is temperature, ν_F is the Fermi velocity, and we included the first three electron and hole sub-bands.

Since our experiments consist of a heterogeneous mixture of nanotube diameters and lengths, we model this as an effective,

ensemble average capacitance, which depends only on the average chemical potential of all the nanotubes.

$$C_q(\mu) = \int dd\ \mathcal{N}(d_0, \Delta d)\ C_q(\mu, d) \tag{11}$$

The mean diameter of the SWNTs we used is 1.4 nm and it varies in the range of 1.2−1.7 nm. We assume a Gaussian distribution (mean at 1.4 nm and deviation at 0.25 nm) to represent the diameter distribution of the SWNTs within the network. From that, we can estimate the ensemble averaged quantum capacitance of a mixed nanotubes. Figure 8 shows the
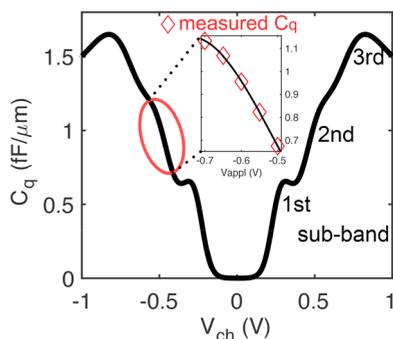

Figure 8. Ensemble averaged quantum capacitance as a function of the change of chemical potential. Ions with close interaction with SWNT can effectively gate SWNT and change its quantum capacitance. The inset curve is the measured quantum capacitance as a function of the liquid gate potential. It fits well with the first and second sub-band of quantum capacitance, considering a shift of V_{ch} due to the choice of reference electrode.

theoretical average quantum capacitance as a function of the chemical potential. Because of the relatively high homogeneity of SWNTs we used, in the calculated C_q curve, we can still see the sub-band structures. For wider range of diameter distribution such as 1−3 nm, the sub-band information will be averaged out and the C_q curve will be simply "V" shaped.

Limitation of Measurement Window. Compared to the theoretical value, the measured quantum capacitance resides in part of the first and second sub-band (red region in Figure 8), corresponding to the applied gate potential −(0.7−0.5) V. The reason we address the capacitance within the limited potential window is that, as potential goes more positive ($V_{appl} > −0.5$ V), the conductance of SWNTs drops exponentially. As shown in the conductance curve (Figure 1), −0.5 V is already in the gray area between the conductive and nonconductive states. With more and more SWNTs disappearing from the measurement circuit, the fraction of SWNTs that contribute to the impedance signal can no longer be determined. Another perspective to verify this is to measure the linearity of the relationship between the measured capacitance and the channel area of SWNT network. In the inset of Figure 2b, when the applied potential goes to -0.5 V, we can see the measurement points start to deviate from the linear relationship. On the other hand, as the potential goes more negative ($V_{appl} < −0.7$ V), redox reaction of electrolyte species will occur and cause a permanent change of the system.

Dependence of C_q on V_{ch}. The measured capacitance consists of not only the quantum capacitance, but also the double layer capacitance in series. In order to compare it with the pure quantum capacitance estimated from the theoretical model, we need to separately determine the quantum

components from the measured total capacitance. The calculation of the double layer capacitance will show that at high ionic strength (e.g., 1 M), the double layer capacitance is large and 1 order of magnitude higher than the quantum capacitance, thus quantum capacitance will be the dominating part of the measured value and double layer part can be neglected, similar to the case of graphene.[24,56] The inset of Figure 8 shows the measured capacitance as a function of the applied potential, which agrees with the theory curve. Note that, at low ionic strength, the double layer capacitance is smaller and cannot be neglected due to its comparable value to the quantum capacitance, hence the measured total capacitance cannot represent the quantum capacitance.

Quantitative Determination of Both Quantum and Electrochemical Capacitances. Now that we have quantitative models for both $C_{dl}(V_{dl})$ and $C_q(V_{ch})$, we can determine the values of V_{dl} and V_{ch} for a given V_{appl} at different electrolyte concentrations. As mentioned above, this determination is done self-consistently using numerical methods. The results are summarized in Figure 9.
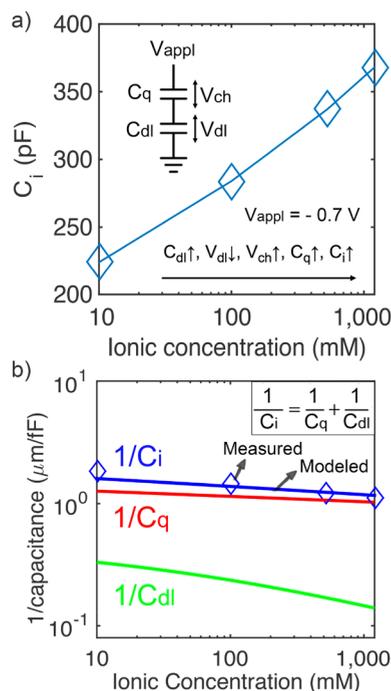

Figure 9. Total interfacial capacitance changes with ionic concentration, caused by potential redistribution between the two types of capacitance. (a) Measured total capacitance of the SWNT−electrolyte interface and (b) modeled total capacitance that includes the quantum capacitance and double layer capacitance.

It is generally known that the double layer capacitance depends on electrolyte concentration, since the Debye screening length changes with the electrolyte concentration.[4] The quantum capacitance, on the other hand, being a property only of the intrinsic density of states, is expected to depend only on the Fermi level, and not the external ionic strength. With this motivation in mind, we measured the ionic strength dependence of the total capacitance.

Figure 9a shows the measured total capacitance of the SWNT-electrolyte interface as a function of the ionic concentration under conditions where the nanotube network

is clearly in the "on-state" (gate potential at −0.7 V). As expected, the data clearly shows a trend of increasing total capacitance with increasing ionic strength: As the ionic strength increases, the Debye length decreases, increasing the double layer capacitance. The prediction in Figure 9b takes into account the modeled double layer capacitance, its dependence on ionic concentration, and its dependence on electrical potential. The applied potential is dropped across both the quantum capacitance and the double layer capacitance. Therefore, for a given applied potential V_{appl}, as the electrolyte concentration changes, the division of V_{appl} between V_{dl} and V_{ch} (Figure 5) changes since the value of C_{dl} changes. For this reason, even for a fixed V_{appl}, V_{ch} changes with ionic strength and therefore the Fermi energy of the electrons in the nanotubes (which depends on V_{ch}) changes, and so does C_q. (C_q is not changing directly as a consequence of the change in the ionic strength.) Therefore, to model the total capacitance at a given bias voltage (as is measured in Figure 5b), it is necessary to self-consistently solve for the total capacitance numerically. Our model, using the experimentally applied voltage in the nanotube on-state, reproduces the ionic concentration dependence well.

Series Model Approximation. We used a series model to account for the relationship between the quantum capacitance and the double layer capacitance. This essentially assumes the interaction between the electrolyte and the nanotube is purely electrostatic, and that the quantum wave functions do not significantly overlap. We now discuss the justification for this model in more detail. First, there is a possibility of charge transfer between the nanotube−electrolyte interface. However, our measurements show this Faradaic current to be negligible. Second, mismatches between the nanotube work function and the electrolyte and reference electrode work functions result simply in an offset to the applied potential. Third, we treat the effect of molecular adsorption as a constant offset to the total applied potential. With all the above assumptions, we can model the total capacitance as $1/C_i = 1/C_q + 1/C_{dl}$. Hence, the combination of the two types of capacitance can be simplified in a series relationship with the smaller one dominating the total capacitance[28] (Figure 5). A similar case was studied on graphite/ionic liquid system, where the electronic state of the electrode plays a role in the total interfacial capacitance, and the two types of capacitance are combined in series relationship.[57]

We turn our attention now to comparison to prior work on small electrodes. In contrast to planar electrodes and ultramicroelectrodes (UMEs), which have been studied both analytically and experimentally in previous work,[4] the total interfacial capacitance of carbon nanotube based electrodes shows qualitatively different behavior arising from the intrinsic quantum capacitance and the geometries of electrodes with extreme curvature and small dimensions. Although the quantum capacitance of individual SWNTs has been evaluated in a dry environment[23] and the double layer capacitance in ionic liquid has been simulated using classical molecular dynamics,[39] this work represents a comprehensive modeling and measurement of these effects in an electrolyte environment. As far as prior experimental data, the overall capacitances of carbon nanotube papers (CNPs) or bulky carbon nanotubes have been measured per gram in previous works;[21,58] however, the capacitance properties of SWNTs were not quantitatively assessed. Heller and co-workers have studied the charge-transfer at the SWNT−electrolyte interface as a function of

band alignment.[28] Our work studies the charge storage instead of charge transfer at the interface. This work provides a comprehensive model of the double layer capacitance of a long, narrow wire. Although it is being applied to the case of carbon nanotubes, it should apply to any long, narrow wire geometry, a case more and more common in modern research on electrochemistry.

CONCLUSION

We developed experimental methods and comprehensive models to investigate SWNT−electrolyte total interfacial capacitance, including the quantum capacitance and electric double layer capacitance. The measured total interfacial capacitance is a combination of two types of capacitance in series: 0.67−1.13 fF/μm for quantum capacitance and 2.3−6.8 fF/μm for double layer capacitance depending on the ionic concentration and applied potential. The obtained quantum capacitance is in consistence with theoretical prediction for SWNTs as well as capacitance measurements in dry environment. SWNTs have critical dimension comparable to ion size. Its double layer capacitance appears quite different from conventional macroscale electrodes. Even though the double layer capacitance of SWNTs is larger than the quantum capacitance and, in many cases, it can be 1 order of magnitude larger, the role of double layer capacitance cannot be neglected. Its sensitivity to ionic concentration can in fact shift the potential distribution across the interface and affects the quantum capacitance. The next logical step to improve on our knowledge and model of the SWNT−electrolyte interface would be to measure directly the impedance of a single nanotube−solution interface. Although it is much more challenging to measure as quantitatively as we have here, such a measurement would provide more comprehensive data on which to base models and theories such as diameter and chirality dependence.

METHODS

SWNT networks were obtained by vacuum filtration of 99.9% purity semiconducting single-walled nanotube ink onto mixed cellulose membrane with 25 nm pore size (MF-Millipore VSWP04700). Then 600 μL of SWNT ink (IsoNanotubes-S 99.9%, diluted in DI water to a concentration of 1 μg/mL) was filtered through the membrane resulting in a uniform coated SWNT network film. Followed by 200 mL DI water rinse to remove residual surfactant, a SWNT network film on mixed cellulose membrane was made and stored for transfer. Soda lime glass was used as the substrate and treated with hot piranha solution for 40 min at 140 °C to achieve a clean surface. Premade SWNT network films were then moistened with ethanol and placed in contact with the cleaned substrate. After 1 h immersion of the device in acetone vapor, most of the mixed cellulose membrane was dissolved and the SWNT network was bonded to the substrate. The residual cellulose was removed in acetone and methanol step by step under carefully tuned conditions (30 min in 60 °C acetone with stir speed 60 rpm and 20 min in methanol at 60 °C with stir speed 60 rpm). After isopropyl alcohol rinse and N_2 gas blow-dry, a large-area uniform SWNT network on glass substrates was made. Device arrays with various channel lengths were then patterned on the SWNT network by a standard photolithography. Ti (2 nm)/Pd (20 nm)/Au (50 nm) were deposited by e-beam evaporation, followed by a lift-off process to form contact electrodes. Oxygen plasma etching was used to constrain the SWNT network within the rectangular channel region between the source electrode and drain electrode. The final step of photolithography was used to open windows in the channel region, leaving the electrodes protected under photoresist polymer and SWNT network exposed.

A PDMS reservoir was then aligned on the device array for delivering aqueous solution. An electrochemical gate potential was applied to the SWNTs with respect to an Ag/AgCl reference electrode that is immersed inside the reservoir, controlled by a potentiostat (Gamry Reference 600). A counter electrode made of platinum was also immersed in the reservoir to form a three-electrode configuration in order to control the liquid gate potential precisely. The potentiostat can apply an AC perturbation at various frequencies superimposed onto the gate potential and monitor the corresponding AC current, from which the EIS was determined. The source-drain conductance was measured by using a source/measure unit (Keysight B2902A) previous to the EIS measurement to eliminate non-conducting devices. During the measurements, the devices were shielded in a Faraday cage to minimize background noise.

ASSOCIATED CONTENT

Ⓢ Supporting Information

The Supporting Information is available free of charge on the ACS Publications website at DOI: 10.1021/acsnano.8b01427.

> Measurement comparison between liquid-gated SWNTs and oxide-gated SWNTs, redox leakage current of SWNT networks, double layer capacitance calculation, density estimation of SWNTs, low frequency approximation, parasitic impedance vs the area of electrode pads, double layer capacitance as a function of ionic concentration, charge storage outside the surface of a cylindrical electrode vs inside an ultranarrow pore (PDF)

AUTHOR INFORMATION

Corresponding Author
*E-mail: pburke@uci.edu.

ORCID Ⓘ
Peter J. Burke: 0000-0002-8883-1014

Notes
The authors declare no competing financial interest.

ACKNOWLEDGMENTS

REFERENCES

(1) Chen, T.; Peng, H.; Durstock, M.; Dai, L. High-Performance Transparent and Stretchable All-Solid Supercapacitors Based on Highly Aligned Carbon Nanotube Sheets. *Sci. Rep.* **2015**, *4*, 3612.

(2) Dunn, B.; Kamath, H.; Tarascon, J.-M. Electrical Energy Storage for the Grid: A Battery of Choices. *Science* **2011**, *334*, 928−935.

(3) Yang, N.; Chen, X.; Ren, T.; Zhang, P.; Yang, D. Carbon Nanotube Based Biosensors. *Sens. Actuators, B* **2015**, *207*, 690−715.

(4) Bard, A. J.; Faulkner, L. R. *Electrochemical Methods: Fundamentals and Applications*, 2nd ed.; John Wiley & Sons, Inc.: New York, 2000.

(5) Wang, H.; Pilon, L. Accurate Simulations of Electric Double Layer Capacitance of Ultramicroelectrodes. *J. Phys. Chem. C* **2011**, *115*, 16711−16719.

(6) Brown, M. A.; Goel, A.; Abbas, Z. Effect of Electrolyte Concentration on the Stern Layer Thickness at a Charged Interface. *Angew. Chem., Int. Ed.* **2016**, *55*, 3790−3794.

(7) Béguin, F.; Frackowiak, E. *Carbons for Electrochemical Energy Storage and Conversion Systems*; CRC Press: Boca Raton, FL, 2010.

(8) Simon, P.; Gogotsi, Y. Materials for Electrochemical Capacitors. *Nat. Mater.* **2008**, *7*, 845−854.

(9) Simon, P.; Gogotsi, Y. Charge Storage Mechanism in Nanoporous Carbons and Its Consequence for Electrical Double Layer Capacitors. *Philos. Trans. R. Soc., A* **2010**, *368*, 3457−3467.

(10) Forse, A. C.; Merlet, C.; Griffin, J. M.; Grey, C. P. New Perspectives on the Charging Mechanisms of Supercapacitors. *J. Am. Chem. Soc.* **2016**, *138*, 5731−5744.

(11) Kondrat, S.; Kornyshev, A. A. Pressing a Spring: What Does It Take to Maximize the Energy Storage in Nanoporous Supercapacitors? *Nanoscale Horiz* **2016**, *1*, 45−52.

(12) Rochester, C. C.; Kondrat, S.; Pruessner, G.; Kornyshev, A. A. Charging Ultrananoporous Electrodes with Size-Asymmetric Ions Assisted by Apolar Solvent. *J. Phys. Chem. C* **2016**, *120*, 16042−16050.

(13) Chmiola, J.; Yushin, G.; Gogotsi, Y.; Portet, C.; Simon, P.; Taberna, P. L. Anomalous Increase in Carbon Capacitance at Pore Sizes Less Than 1 Nanometer. *Science* **2006**, *313*, 1760−1763.

(14) Lee, A. A.; Kondrat, S.; Kornyshev, A. A. Single-File Charge Storage in Conducting Nanopores. *Phys. Rev. Lett.* **2014**, *113*, 048701.

(15) Kornyshev, A. A. The Simplest Model of Charge Storage in Single File Metallic Nanopores. *Faraday Discuss.* **2013**, *164*, 117−133.

(16) Kondrat, S.; Kornyshev, A. Corrigendum: Superionic State in Double-Layer Capacitors with Nanoporous Electrodes. *J. Phys.: Condens. Matter* **2013**, *25*, 119501.

(17) Kondrat, S.; Georgi, N.; Fedorov, M. V.; Kornyshev, A. A. A Superionic State in Nano-Porous Double-Layer Capacitors: Insights from Monte Carlo Simulations. *Phys. Chem. Chem. Phys.* **2011**, *13*, 11359−11366.

(18) Kondrat, S.; Wu, P.; Qiao, R.; Kornyshev, A. A. Accelerating Charging Dynamics in Subnanometre Pores. *Nat. Mater.* **2014**, *13*, 387−393.

(19) Chen, H.; Zeng, S.; Chen, M.; Zhang, Y.; Li, Q. Fabrication and Functionalization of Carbon Nanotube Films for High-Performance Flexible Supercapacitors. *Carbon* **2015**, *92*, 271−296.

(20) Malik, R.; Zhang, L.; McConnell, C.; Schott, M.; Hsieh, Y. Y.; Noga, R.; Alvarez, N. T.; Shanov, V. Three-Dimensional, Free-Standing Polyaniline/Carbon Nanotube Composite-Based Electrode for High-Performance Supercapacitors. *Carbon* **2017**, *116*, 579−590.

(21) Barisci, J. N.; Wallace, G. G.; Baughman, R. H. Electrochemical Studies of Single-Wall Carbon Nanotubes in Aqueous Solutions. *J. Electroanal. Chem.* **2000**, *488*, 92−98.

(22) Rutherglen, C.; Burke, P. Nanoelectromagnetics: Circuit and Electromagnetic Properties of Carbon Nanotubes. *Small* **2009**, *5*, 884−906.

(23) Ilani, S.; Donev, L. A. K.; Kindermann, M.; McEuen, P. L. Measurement of the Quantum Capacitance of Interacting Electrons in Carbon Nanotubes. *Nat. Phys.* **2006**, *2*, 687−691.

(24) Xia, J.; Chen, F.; Li, J.; Tao, N. Measurement of the Quantum Capacitance of Graphene. *Nat. Nanotechnol.* **2009**, *4*, 505−509.

(25) Xu, H.; Zhang, Z.; Peng, L.-M. Measurements and Microscopic Model of Quantum Capacitance in Graphene. *Appl. Phys. Lett.* **2011**, *98*, 133122.

(26) Rouhi, N.; Jain, D.; Burke, P. J. High-Performance Semiconducting Nanotube Inks: Progress and Prospects. *ACS Nano* **2011**, *5*, 8471−8487.

(27) Bisquert, J. Theory of the Impedance of Electron Diffusion and Recombination in a Thin Layer. *J. Phys. Chem. B* **2002**, *106*, 325−333.

(28) Heller, I.; Kong, J.; Williams, K. A.; Dekker, C.; Lemay, S. G. Electrochemistry at Single-Walled Carbon Nanotubes: The Role of Band Structure and Quantum Capacitance. *J. Am. Chem. Soc.* **2006**, *128*, 7353−7359.

(29) Brug, G. J.; van den Eeden, A. L. G.; Sluyters-Rehbach, M.; Sluyters, J. H. The Analysis of Electrode Impedances Complicated by the Presence of a Constant Phase Element. *J. Electroanal. Chem. Interfacial Electrochem.* **1984**, *176*, 275−295.

(30) Bisquert, J.; Garcia-Belmonte, G.; Bueno, P.; Longo, E.; Bulhões, L. O. S. Impedance of Constant Phase Element (CPE)-Blocked Diffusion in Film Electrodes. *J. Electroanal. Chem.* **1998**, *452*, 229−234.

(31) Shoar Abouzari, M. R.; Berkemeier, F.; Schmitz, G.; Wilmer, D. On the Physical Interpretation of Constant Phase Elements. *Solid State Ionics* **2009**, *180*, 922−927.

(32) Pajkossy, T. Impedance of Rough Capacitive Electrodes. *J. Electroanal. Chem.* **1994**, *364*, 111−125.

(33) Henstridge, M. C.; Dickinson, E. J. F.; Compton, R. G. On the Estimation of the Diffuse Double Layer of Carbon Nanotubes Using Classical Theory: Curvature Effects on the Gouy-Chapman Limit. *Chem. Phys. Lett.* **2010**, *485*, 167−170.

(34) Leiva, E. P. M.; Sánchez, C. G.; Vélez, P.; Schmickler, W. Theory of Electrochemical Monoatomic Nanowires. *Phys. Rev. B: Condens. Matter Mater. Phys.* **2006**, *74*, 035422.

(35) Maribo-Mogensen, B.; Kontogeorgis, G. M.; Thomsen, K. Comparison of the Debye−Hückel and the Mean Spherical Approximation Theories for Electrolyte Solutions. *Ind. Eng. Chem. Res.* **2012**, *51*, 5353−5363.

(36) Loehe, J. R.; Donohue, M. D. Recent Advances in Modeling Thermodynamic Properties of Aqueous Strong Electrolyte Systems. *AIChE J.* **1997**, *43*, 180−195.

(37) Henderson, D.; Jiang, D.; Jin, Z.; Wu, J. Application of Density Functional Theory To Study the Double Layer of an Electrolyte with an Explicit Dimer Model for the Solvent. *J. Phys. Chem. B* **2012**, *116*, 11356−11361.

(38) Kornyshev, A. A.; Partenskii, M. B.; Schmickler, W. Self-Consistent Density Functional Approach to a Metal/Electrolyte Solution Interface. *Z. Naturforsch., A: Phys. Sci.* **1984**, *39*, 1122−1133.

(39) Pak, A. J.; Paek, E.; Hwang, G. S. Relative Contributions of Quantum and Double Layer Capacitance to the Supercapacitor Performance of Carbon Nanotubes in an Ionic Liquid. *Phys. Chem. Chem. Phys.* **2013**, *15*, 19741−19747.

(40) Hatlo, M. M.; van Roij, R.; Lue, L. The Electric Double Layer at High Surface Potentials: The Influence of Excess Ion Polarizability. *Europhys. Lett.* **2012**, *97*, 28010.

(41) Bagotsky, V. S. *Fundamentals of Electrochemistry*, 2nd ed.; John Wiley & Sons, Inc.: Hoboken, NJ, 2005.

(42) Goodwin, Z. A. H.; Feng, G.; Kornyshev, A. A. Mean-Field Theory of Electrical Double Layer In Ionic Liquids with Account of Short-Range Correlations. *Electrochim. Acta* **2017**, *225*, 190−197.

(43) Mohammadzadeh, L.; Quaino, P.; Schmickler, W. Interactions of Anions and Cations in Carbon Nanotubes. *Faraday Discuss.* **2016**, *193*, 415−426.

(44) Schmickler, W.; Henderson, D. Charge Storage in Nanotubes: The Case of a 2−1 Electrolyte. *Condens. Matter Phys.* **2017**, *20*, 33004.

(45) Schmickler, W.; Henderson, D. On the Capacitance of Narrow Nanotubes. *Phys. Chem. Chem. Phys.* **2017**, *19*, 20393−20400.

(46) Mohammadzadeh, L.; Goduljan, A.; Juarez, F.; Quaino, P.; Santos, E.; Schmickler, W. Nanotubes for Charge Storage − towards an Atomistic Model. *Electrochim. Acta* **2015**, *162*, 11−16.

(47) Goduljan, A.; Juarez, F.; Mohammadzadeh, L.; Quaino, P.; Santos, E.; Schmickler, W. Screening of Ions in Carbon and Gold Nanotubes — A Theoretical Study. *Electrochem. Commun.* **2014**, *45*, 48−51.

(48) Schmickler, W. A Simple Model for Charge Storage in a Nanotube. *Electrochim. Acta* **2015**, *173*, 91−95.

(49) Rochester, C. C.; Pruessner, G.; Kornyshev, A. A. Statistical Mechanics of "Unwanted Electroactuation" in Nanoporous Supercapacitors. *Electrochim. Acta* **2015**, *174*, 978−984.

(50) Burt, R.; Birkett, G.; Zhao, X. S. A Review of Molecular Modelling of Electric Double Layer Capacitors. *Phys. Chem. Chem. Phys.* **2014**, *16*, 6519−6538.

(51) Kilic, M. S.; Bazant, M. Z.; Ajdari, A. Steric Effects in the Dynamics of Electrolytes at Large Applied Voltages. I. Double-Layer Charging. *Phys. Rev. E* **2007**, *75*, 021502.

(52) Nightingale, E. R. Phenomenological Theory of Ion Solvation. Effective Radii of Hydrated Ions. *J. Phys. Chem.* **1959**, *63*, 1381−1387.

(53) Butt, H.; Graf, K.; Kappl, M. *Physics and Chemistry of Interfaces*; Wiley-VCH: New York, 2003.

(54) Gavryushov, S.; Linse, P. Polarization Deficiency and Excess Free Energy of Ion Hydration in Electric Fields. *J. Phys. Chem. B* **2003**, *107*, 7135−7142.

(55) Liang, J.; Akinwande, D.; Wong, H.-S. P. Carrier Density and Quantum Capacitance for Semiconducting Carbon Nanotubes. *J. Appl. Phys. (Melville, NY, U. S.)* **2008**, *104*, 064515.

(56) Wang, Y. Y.; Pham, T. D.; Zand, K.; Li, J.; Burke, P. J. Charging the Quantum Capacitance of Graphene with a Single Biological Ion Channel. *ACS Nano* **2014**, *8*, 4228−4238.

(57) Kornyshev, A. A.; Luque, N. B.; Schmickler, W. Differential Capacitance of Ionic Liquid Interface with Graphite: The Story of Two Double Layers. *J. Solid State Electrochem.* **2014**, *18*, 1345−1349.

(58) Yang, Z.; Wu, H. The Electrochemical Impedance Measurements of Carbon Nanotubes. *Chem. Phys. Lett.* **2001**, *343*, 235−240.

Carbon Nanotube-Electrolyte Interface: Quantum and Electric Double Layer Capacitance

Jinfeng Li,[†] Phi H. Q. Pham,[‡] Weiwei Zhou,[§] Ted D. Pham,[‖] and Peter J. Burke[*,‡,§,‖,⊥]

[†]Department of Physics and Astronomy, [‡]Department of Chemical Engineering and Materials Science, [§]Integrated Nanosystems Research Facility, [‖]Department of Biomedical Engineering, and [⊥]Department of Electrical Engineering and Computer Science, University of California, Irvine, California 92697, United States

Supplementary Note 1: _Measurement comparison between this work and the reference work_

	C_{total} (fF/µm)	C_{gate} (fF/µm)	C_q (fF/µm) - 1st subband	C_q (fF/µm) - 2nd subband
Ref. [1]	~0.06	0.0615	0.5~0.8	N/A
This work	0.9	2~7	0.67~1.16	

Here, we compare a liquid-gated carbon nanotube (this work) versus oxide-gated carbon nanotube (reference work[1]). In both cases, the measured total capacitance contains two capacitances in series: the gate capacitance (C_{gate}) and the carbon nanotube intrinsic quantum capacitance (C_q). The total capacitance takes the form, $1/C_{total}=1/C_{gate}+1/C_q$. The main difference between our work and the reference work is in the term, C_{gate}. In the reference work, C_{gate} is determined by the geometry and dielectric constant of the oxide layer between the gate electrode and the carbon nanotube, which, as evaluated in the reference work, is a constant value of 61.5 aF/µm. However, in our case, C_{gate} is the double layer capacitance, which is a non-trivial function of the surface potential and ionic strength. This term has not been thoroughly studied in the case of nanoscale 1d nanotube, and presents a major difference in the capacitance measurement.

Despite the difference on C_{gate}, the intrinsic C_q should be the same for both cases. The reference work presents the capacitance data (C_{nt}) only as a total quantity, and does not give directly, C_q. However, from the given value of the gate capacitance, 61.5 aF/µm, and the g-

parameter (which is the square root of the ratio between the total capacitance and quantum capacitance), ~ 0.26 - 0.34, we can calculate C_q, which yields a value ranging ~ 0.5 - 0.8 fF/μm for the 1st sub-band. This value should be expected to be larger in the 2nd sub-band. Our work measures C_q over both the 1st and 2nd sub-band and gives value of ~ 0.67 - 1.16 fF/μm. Therefore, our measured value indeed does agree with the capacitance value as reported in the referenced work.

Supplementary Note 2: Redox leakage current of SWNT networks

Figure S1 shows the gate leakage current vs. gate potential. The leakage current is less than 0.4 nA within the liquid gate potential window, about one order of magnitude less than the source-drain current. This indicates that top layer photoresist can effectively insulate the source/drain electrodes and the charge transfer current is small enough to be ignored.
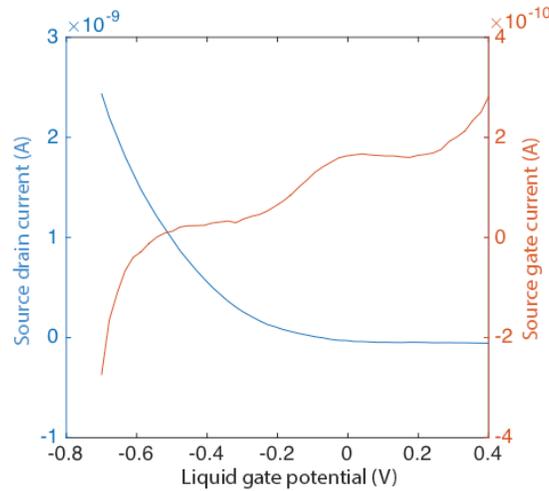

Figure S1: Source drain current and gate leakage current

Supplementary Note 3: Double layer capacitance calculation

According to Gauss's law, the accumulated net charge in the screening layers can be calculated,

$$q^{screen} = \varepsilon\varepsilon_0 \oiint_{\substack{Gauss \\ Surface}} \vec{E} \cdot \overrightarrow{dS} = \varepsilon\varepsilon_0(2\pi r_1 L)\frac{\partial\varphi}{\partial r}|_{r=r_1} \tag{S1}$$

where L is the length of the electrode. Screening charge counter-balances the net charge in the electrode, so $q^{SWNT} = -q^{screen}$. The double layer capacitance is the derivative of the net charge as a function of the electrode potential, *i.e.* $C_{dl} = dq^{SWNT}/d\varphi_0$.

Supplementary Note 4: SWNT density estimation

The density of SWNTs is estimated from the SEM image. Assuming a straight line with enough length lying on the SWNT network sheet, the probability of a single nanotube with length of l crossing the straight line is:

$$P_i = 2 \int_0^{l/2} \frac{2 \, Cos^{-1}[2x/l]}{b \, \pi} \, dx = \frac{2 \, l}{b \, \pi} \tag{S2}$$

where b is the width of the SWNT network sheet. Then the SWNT density of the sheet will be:

$$density \; of \; SWNT = N \cdot \frac{\pi}{2 \, l} \tag{S3}$$

where N is the average number of SWNTs that cross the line within a unit length.

By placing 5μm lines randomly on the SEM image of the TFT devices and counting the SWNTs that cross the lines, we can estimate N ≈ 8. The SWNTs used in this experiment are commercially available from Nanointegris, and it have mean diameter of 1.4 nm and mean length of *l=1μm*. About 12.6 SWNTs per unit area can be estimated for the SWNTs density.

Supplementary Note 5: Low frequency approximation

The capacitance calculation using a RC series circuit model only works well in limited condition. As we can see in figure S2, only in the on state (red curve) and low frequency range (below ~100 Hz), the real capacitance spectrum has less dependence on frequency. In the off state (blue curve), even at very low frequency, the real capacitance shows no sign of leveling off. Therefore, when measuring the SWNT-electrolyte capacitance at 10 Hz (figure 2a), as the potential goes in the direction to off state, the calculated capacitance can no longer represent the true capacitance. This is also a reason we can only estimate the potential dependence in a small range.
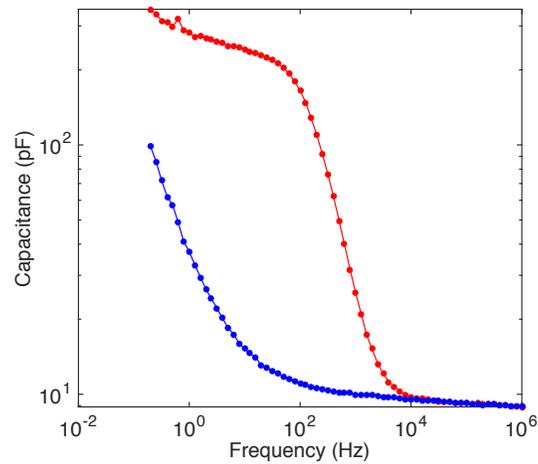
Figure S2: real capacitance spectrum of SWNT network at on state (red) and off state (blue).

Supplementary Note 6: *Parasitic impedance vs. the area of electrode pads*

Figure S3 shows the strong correlation between the electrode area and the impedance at high frequency (1 MHz). The areas estimation only takes account of the regions of electrodes that are underneath the electrolyte solution. This strong correlation confirms that parasitic current of the device mainly passes from the electrode to the solution through the protective dielectric layer. Hence, the parasitic impedance should be in parallel with the impedance of the SWNT-electrolyte interface.
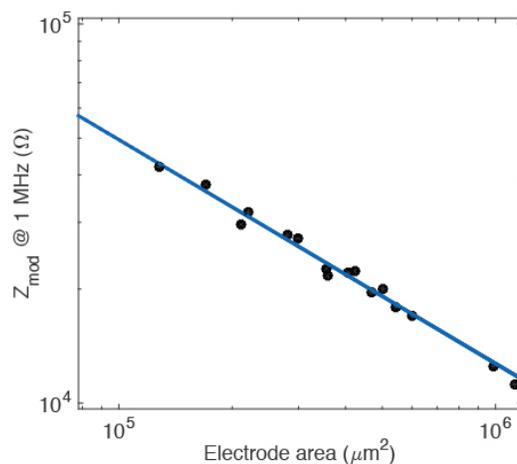

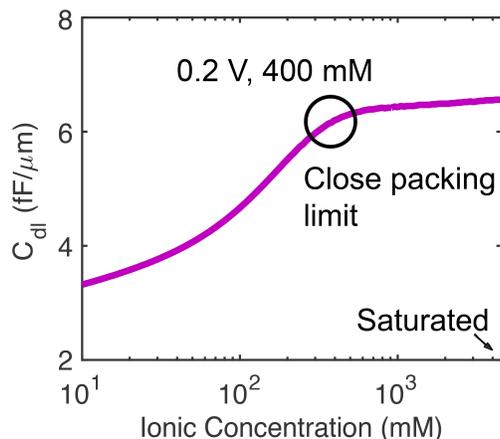*Figure S3: The impedance modulus at high frequency vs. the electrode pad areas.*

Figure S4: Double layer capacitance as a function of ionic concentration. The capacitance reaches close-packing limit at ionic concentration ~400 mM and surface potential 0.2 V.

Increasing ionic concentration has a similar effect on the C_{dl} as increasing surface potential. As shown in figure S4, the C_{dl} first increases and then reaches a limit when ions start close-packing. However due to the extreme convex curvature of SWNTs, there is more space for ion diffusion per surface area than planar electrode. Hence ion close-packing happens in higher surface potential or higher ionic concentration.

Supplementary Note 8: *Charge storage outside the surface of a cylindrical electrode vs. inside an ultranarrow pore*
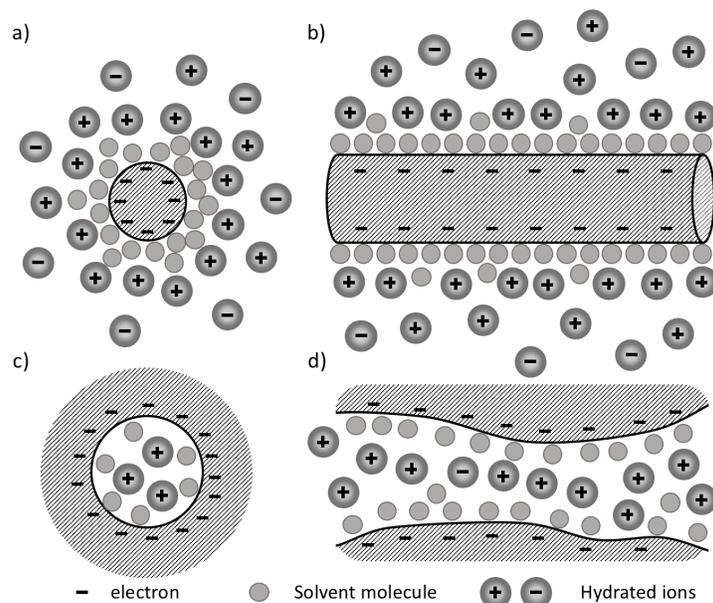

Figure S5: Cartoon diagram showing the different mechanism of charge storage outside the surface of a solid cylindrical electrode (a, b) and inside a ultranarrow pore (c, d)

This diagram is to further clarify the case of our study (a, b) vs nanopore case (c, d). Our sample contains an ultrathin layer of carbon nanotubes sparsely deposited on a flat substrate. The SEM characterization shows that the average nanotube density is ~ 12.6/μm^2, which means the average distance between nanotube is large (~ 100 nm) in the substrate plane and no confinement above the plane. Hence the confinement effect can be ignored. Although the nanotubular pore inside a nanotube can contribute to the total capacitance, this part can also be neglected in the case of our study (nanotube gated at around 0.5 V), because the differential capacitance of the narrow tubular pore is small and vanishes over a threshold potential. The differential capacitance is small because, once the inner portion of the nanotube is filled up with ionic charge, it is "full", and adding additional voltage will not increase the charge.

Reference:

(1) Ilani, S.; Donev, L. A. K.; Kindermann, M.; McEuen, P. L. Measurement of the Quantum Capacitance of Interacting Electrons in Carbon Nanotubes. *Nat. Phys.* **2006**, *2*, 687–691.